J Therm Anal Calorim (2009) 97:289–296
DOI 10.1007/s10973-009-0259-1

Complexation of the Fe(III) and Fe(II) sulphates with diphenyl-4-amine barium sulphonate (DAS) Synthesis, thermogravimetric and spectroscopic studies

L. C. Machado · A. A. L. Marins · E. J. B. Muri · A. Biondo · J. do R. Matos · I. O. Mazali

ICTAC2008 Conference

Abstract Reactions in aqueous-alcoholic solution between diphenyl-4-amine barium sulphonate (Ba-DAS—anionic surfactant) and the hydrated sulphates of Fe(III) and Fe(II) ions and their use to ovtain iron oxides are described here. The formation of Fe(II) complexes was reached by using an excess of Ba-DAS, in absence of light under inert atmosphere. The complexes achieved $Fe_2[(C_{12}H_{10}NO_3S)_4]\cdot 9H_2O$ and $Fe_3[(C_{12}H_{10}NO_3S)_6]\cdot 12H_2O$ were characterized by TG/DTG and IR, UV-VIS and ^{57}Fe-Mössbauer analyses.

Keywords Hematite · Magnetite · Synthesis · Sulphonate

Introduction

Reduction of the particle size of Fe_2O_3 and Fe_3O_4 oxides to nanometric scale can be useful in some technological aspects. Nevertheless, for such specification level, standardizing the experimental conditions of sample preparation is essential [1–5], which e.g., prevents the formation of microstructured oxide particles with different crystallinities exhibiting similar sizes and shapes. These requirements are more distinguishable for some oxide properties such as superparamagnetism, quantum tunneling of magnetization, and large coercivities, which are revealed only when the particles attain sizes under a determined critical value [2, 4, 5]. For Fe_3O_4, the methods described are various, such as precipitation in the presence of polyvinyl alcohol, chemical reduction of α-Fe_2O_3, decomposition of oxalates, citrates and hydroxides [3–6]. Production of α-Fe_2O_3 nanoparticles involves from application of thermal transformations of metallic iron under oxidizing atmospheres, thermal oxidation of Fe_3O_4, iron salts hydrolysis until the use of surfactants containing large carboxylate alkyl chains [1, 2, 5, 7, 8]. Surfactants act in order to prevent the aggregation of α-Fe_2O_3 nanoparticles into clusters generated by the anisotropy of the dipolar attraction, which, by changing, causes loss of properties associated to the single domain. In the last years, successful protection of α-Fe_2O_3 nanoparticles have sometimes been achieved by using anionic alkyl-sulphonate surfactants such as dodecylbenzene sulphonate and 1-undecane sulphonic acid, besides 1-octanol (alcohol) [7]. It has been emphasized that surfactants may stabilize the morphology of Fe_3O_4, even though it depends on the initial amount of Fe(II) present in the process. However, particle sizes are between 2 and 20 nm in order to control these factors. Despite the advances, the points of view are not unanimous about the exact role of surfactants [1, 7]. Some inconveniences from the use of surfactants have been pointed out due to the difference on the interaction between the latter and the surface and inside of the particles [1]. According to this point of view, anionic surfactants interact less strongly

L. C. Machado (✉) · A. A. L. Marins · E. J. B. Muri
LPNM-DQUI, UFES, Av. Fernando Ferrari, 574, Vitória, ES 29075-910, Brazil
e-mail: lcmachado123@yahoo.com.br

A. Biondo
DFIS, UFES, Av. Fernando Ferrari, 574, Vitória, ES 29075-910, Brazil

J. d. R. Matos
LATIG-IQ-USP, Av. Prof. Lineu Prestes 748, Bloco 8T, São Paulo, SP 05508-000, Brazil

I. O. Mazali
LQES-IQ-UNICAMP, CP 6154, Campinas, SP 13084-971, Brazil

with oxygen bonded to Fe on the surface of particles, modifying less the original bond length. Under these conditions, there aren't variations between atomic vibrations between the center and the surface of particles, TEM and EXAFS data suggest that cationic surfactants, differently, attach to the oxygen atom and increase significantly the bond length (Fe–O) on the surface, ordering the nanoparticles and suppressing the atomic vibrations on the particle surface. The anharmonicity of the nanoparticles can be associated to this difference in the bond characteristics between center and surface atoms [1, 2, 4].

Here, the reactions in water—alcohol solution mixtures between diphenyl-4-amine barium sulphonate surfactant and iron (II) and iron (III) hydrate sulphates were studied aiming to obtain precursor complexes for the iron oxides. The interaction between anionic ligand and iron ions will be investigated here, as well as the coordination characteristics, thermal stability, binding site, conductivity in solution and type and characteristics of the produced complexes and oxides.

Nevertheless, the formation reaction of the complexes with the anionic surfactant DAS must include procedures that control the surfactant's oxidizing photodegradation, catalyzed by Fe(III) ions. In this degradation process, the surfactant and Fe(III) ion complex absorbs light inside the visible spectral region. The excited ligand radical $L^{\bullet +}$ in general reaches its most stable oxidation state through an intermolecular process that reduces the Fe(III) to Fe(II). Radiations with $\lambda > 330$ nm are enough for the ligand excitation [9–13].

If Fe(III) ion is not complexed to the ligand/surfactant, it reacts with the water molecules. Among the species hydrolyzed in aqueous solutions of Fe(III) (pH = 2.5–4.0) $Fe(OH)^{2+}$ form dominates and is characterized by high photo activity at $\lambda = 313$ and 365 nm. If irradiated, the species $Fe(OH)^{2+}$ acts as a photodegradation starter through the internal transfer of electrons, which photo reduces the $Fe(OH)^{2+}$ species, producing the Fe(II) ions and the $^{\bullet}OH$ radical [9, 11, 12].

In general, the oxidation reactions catalyzed by Fe(III) have always been limited to the photo-oxidizing effects of the hydrolyzed species, such as $Fe(OH)^{2+}$ ion, discarding the role of organic ligand. However, organic ligands influence the chemistry of the iron redox processes [12, 13]. In the present work Fe(III) was complexed with a sulfate anion according to (1):

$$3Ba(DAS)_{2(aq)} + Fe_2(SO_4)_{3(aq)} \rightarrow 3BaSO_{4(S)} + Fe_2(DAS)_{4(aq)} + 2(DAS)_{oxid} \quad (1)$$

The competition established is limited to the reducing species SO_3R^- and to the highly coordinating SO_4^{2-}. Only with the reaction progress and the consumption of sulphate ion producing $BaSO_4$, the SO_3R^- anion starts to reduce Fe(III) to Fe(II) [13]. For comparison, product of reaction 2 will receive the same care.

$$3Ba(DAS)_{2(aq)} + 3\ Fe(SO_4)_{(aq)} \rightarrow 3BaSO_{4(S)} + Fe_3(DAS)_{6(aq)} \quad (2)$$

Experimental

Synthesis of Fe_xDAS_{2x} complexes

The synthesis of Fe_xDAS_{2x} complexes ($x = 2$ or 3) involves the slow addition of aqueous solutions of the hydrated sulphates of Fe(II) and Fe(III) to water/ethanol 7:1 solutions containing Ba-DAS at 60 °C under inert atmosphere, the exclusion of light and with constant agitation until total precipitation of $BaSO_4$. The final precipitate was filtered and washed several times with purified hexane.

Obtainment of iron oxides from the Fe_xDAS_{2x} complexes

The Fe_xDAS_{2x} complexes are thermal treated in a muffle type furnace up to 1000 °C, at a heating rate of 10 °C min^{-1} under air.

Characterization of the Fe_xDAS_{2x} complexes and the iron oxides

Carbon, hydrogen and nitrogen contents of the complexes were determined using PerkinElmer 2400(CHN) equipment. Spectra of solutions at 10^{-4} mol L^{-1} concentratios of the iron complexes were obtained in the UV-VIS range using a Varian spectrophotometer model Cary 1E. IR spectra were recorded in a FTIR Bomem MB 100 in the 350–4000 cm^{-1} operation range, in KBr pellets.

TG/DTG curves of Fe complexes were obtained in a Shimadzu TGA-50H equipment under dynamic O_2 and N_2 atmospheres (60 mL min^{-1}) and at a heating rate of 10°C min^{-1} from room temperature up to 1000 °C. X-ray diffractograms (XRD) of the iron oxides were obtained in a HZG diffractometer with quartz monochromator for Kα of Co ($\lambda = 1.79020$ Å) radiation line.

The ^{57}Fe Mössbauer spectra of the Fe_xDAS_{2x} complexes were obtained in an energy modulation system through Doppler Effect of the ^{57}Fe δ radiation (^{57}Co isotope source). The δ energy modulation system comprises a Mössbauer velocity transducer, a driving system and a function generator.

Results and discussion

Synthesis and characterisation of Fe_xDAS_{2x} complexes

Ba-DAS solubilization occurred at 60 °C after ethanol addition, in a ratio of 1:7 in relation to the aqueous solution volume. Besides improving solubility of DAS-Ba in water, the addition of purified ethanol to the solution makes the photo degradation of the surfactant by the Fe(III) ion more difficult. The Fe(III) ions, even when complexed by the sulphate ion, are still susceptible to a slow hydrolysis that generates the photo active species $Fe(OH)^{2+}$ or to the photodegradation by the anion $SO_3\dot{R}$. The addition of alcohol inhibits these processes. This care, the sulphate ion, the excess of surfactant, the inert atmosphere and the temperature and pH (<5) control minimize the action of the oxidizing species [5, 9, 11–13].

The blue solid produced by reaction 1 (complex A, Fe_2DAS_4) was characterized as $[Fe_2(C_{12}H_{10}NO_3S)_4]\cdot 9H_2O$ (1265.6 g/mol) and yield over 64%. The greenish product obtained in reaction 2 (complex B, Fe_3DAS_6) with yield over 70% calculated from $[Fe_3(C_{12}H_{10}NO_3S)_6]\cdot 12H_2O$ (1871.4 g/mol), Table 1.

Figure 1 shows UV-Vis spectra of BA-DAS and of both Fe(II) complexes. The maximum of the spectra is close to $\lambda = 246$ nm, normally attributed to the transition of π electrons and associated to the displacement of double bond inside the aromatic rings. The small difference found between the λ_{max} of the Ba-DAS and the Fe(II) complexes and the band intensities indicate that the ions are slight affected by the DAS ligand [9, 11]. The reactions destined to the ligand photo degradation catalyzed by Fe(III) use $\lambda = 365$ nm for the excitation of the photo active species $FeOH^{2+}$. In this study, however, it was impossible to attribute a band to this species in the UV-Vis spectra [9, 11–13].

Figure 2 shows the infrared spectra of Ba-DAS, and Fe_2DAS_4 and Fe_3DAS_6 complexes. Table 2 presents the attempts to attribute the bands of the IR spectra of the

Table 1 Analytical results for elemental composition and Mössbauer spectroscopy parameters of the complexes A $[Fe_2(C_{12}H_{10}NO_3S)_4]\cdot 9H_2O$ (Fe_2DAS_4) and B $[Fe_3(C_{12}H_{10}NO_3S_2)_6]\cdot 12H_2O(Fe_3DAS_6)$

Complexes	$Fe_3(C_{12}H_{10}NO_3S_2)_6\cdot 12H_2O$	$Fe_2(C_{12}H_{10}NO_3S)_4\cdot 9H_2O$
C	46.31 (46.17)*	45.57(45.53)*
H	4.52 (4.49)*	4.45 (4.58)*
N	4.08 (4.48)*	4.30 (4.42)*
Fe	8.75 (8.95)*	8.64 (8.82)*
δ (mm/s)	1.261	1.282
ΔE_Q (mm/s)	3.053	2.937
Λ (μS/s)	180.0	142.6

* calculated data

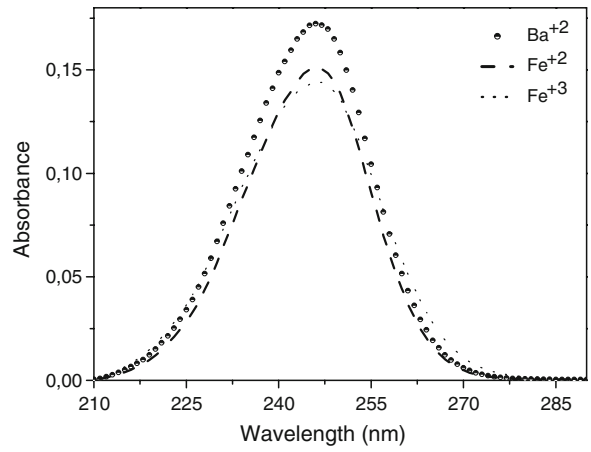

Fig. 1 UV-Vis spectra of the ligand $Ba(C_{12}H_{10}NO_3S)_2$ and Iron (II) complexes (A and B)

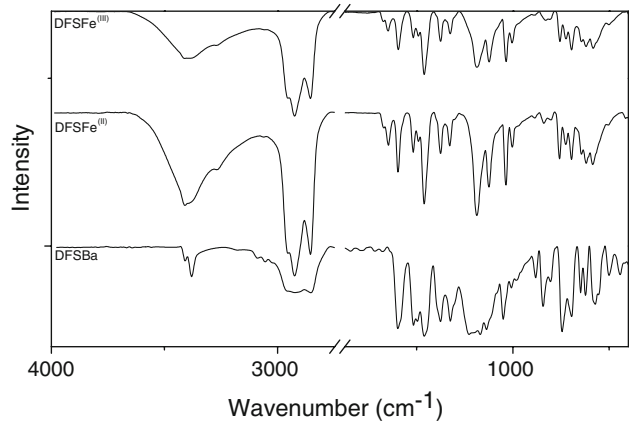

Fig. 2 IR spectra of the ligand $Ba(C_{12}H_{10}NO_3S)_2$ and complexes A and B

Table 2 Infrared data attributions for the ligand (DAS-Ba) and complexes A $(DAS\text{-}Fe)_{red}$ and B (DAS-Fe)

	Ligand	Complex A	Complex B
Stretching C=C	1597 (vs)	1595 (m)	1597(m)
	1580 (sh)	–	–
	1516 (sh)	1518 (w)	1518 (w)
	1420 (vs)	–	–
Bending CH_3 symmetrical	1377 (s)	1375 (w)	1375 (m)
Stretching CN	1325 (s)	1325 (m)	1329 (m)
Stretching $(R–SO_3)^-$	1228 (sh)	–	–
	1184 (sh)	1188 (s)	1188 (s)
	1051 (s)	1036 (s)	1036 (s)
Bending C–H Aromatic	1138 (sh)	1124 (s)	1124 (s)
	1008 (w)	1005 (w)	1003 (w)
	843 (s)	829 (w)	839 (w)

vs very strong, *s* strong, *w* weak, *m* medium, *sh* shoulder

complexes [14–18]. The analysis of the IR spectra, before and after complexation allows identifying the complexation process of the Fe(II) ions by DAS. The bands attributed to the stretching of the aromatic C=C bond appear in ligand spectrum at 1597, 1580, 1516 and 1420 cm^{-1} decrease significantly after complexation. However, this effect is much stronger for the band at 1580 cm^{-1}, typical of the ring conjugation, but that practically disappears in the spectra of both complexes. The bands associated to torsion in and outside the C–H aromatic bond plans appear at 1138, 1008 and 843 cm^{-1} in the ligand, remaining with weak intensities in the complexes spectra [14, 17, 18]. The most important change in the IR spectra and associated to the complexation process refers to the bands attributed to the sulphonate group ($R–SO_3^-$)of the DAS ligand. The 1229, 1184 and 1051 cm^{-1} bands appearing in the ligand spectrum are usually associated to (doubly degenerate) asymmetric and symmetric stretching of the sulphonate group that shows symmetry C_{3V}. With the complex formation, the 1229 cm^{-1} band totally disappears in the spectra. This effect is due to decrease in the symmetry C_{3V} in the complexes, which removes the double degeneration of the asymmetric stretching of the group and lowers the symmetry of the group. The other bands are slightly displaced to frequencies of the symmetric stretching (1036 cm^{-1}) and asymmetric (1188 cm^{-1}) of the group S=O [14–18].

Figure 3 correspond to the Mössbauer spectra of the Fe(II) ion in the two complexes suitable to investigate the coordination sites [3, 15, 19].

The quadrupole splitting parameters (Δ) and isomeric displacement (δ) were obtained from the computer-adjusted spectra of Fig. 3. In Table 1 the Δ and δ values of the Fe(II) ion in both complexes and at room temperature are compared for $FeSO_4{\cdot}7H_2O$ [19]. For both complexes, it was verified a single doublet with the δ values for Fe_2DAS_4 and Fe_3DAS_6 equal 1.282 mm/s and 1.261 mm/s, respectively; and Δ values of 2.937 and 3.053 mm/s, respectively. Comparison with accepted values for $FeSO_4{\cdot}7H_2O$ ($\delta_A = 1.261$ mm/s; $\Delta = 3.217$ mm/s) indicates total reduction of Fe(III) initial (reaction 1). Quantitatively, these values imply that in the complexes the Fe(II) ion occupies the distorted octahedral sites with high spin values [3, 15, 19].

Thermogravimetric Characterization of the Fe_xDAS_{2x} Complexes

The complexes were characterized by TG/DTG under dynamic O_2 and N_2 atmospheres [20–22]. Figure 4 illustrates the evolution of the mass losses occurred in both complexes as temperature increased. The mass loss and the respective residues under different atmospheres are presented in Table 3 (complex A, Fe_2DAS_4) and Table 4

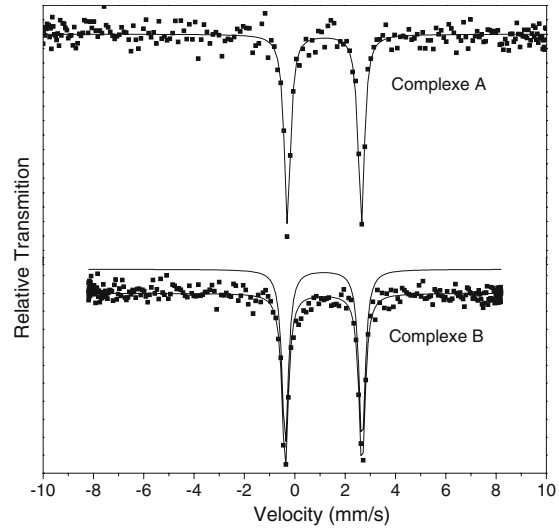

Fig. 3 ^{57}Fe-Mössbauer spectrum of complexes A and B

(complex B, Fe_3DAS_6). Figure 5 contains the scheme illustrating the event temperature intervals and the type of mass losses simulated corresponding to Tables 3(a) and 4(b).

The Fe_2DAS_4 complex presents expressive differences in the mass loss as well as in its respective development for both atmospheres. The first mass loss of 12.30% at $t = 120$ °C (calcd. 12.80%) in N_2 agree with the evaporation of crystallization water. In despite this, in TG/DTG curve under O_2 the first loss was distributed in a larger temperature range (120–480 °C), indicating probably thermal decomposition of compound A as suggested by attribution (15.00%) to the experimental loss (14.71%). For other temperatures the mass losses show differently, i.e., in (O_2), there is higher loss (72.65%) within a shorter temperature range (505–515 °C), whereas under N_2, the mass losses are distributed within the temperature range 400–1000 °C. Although the difference, the final results of the processes result in the residues of 12.62% under O_2 and 12.61% under N_2 corresponding to α-Fe_2O_3. This simulation allow to the calculation of molecular mass of the Fe_2DAS_4 complex as 1264.7 g mol^{-1}(O_2) and 1265.7 g mol^{-1} (N_2) (elemental analysis 1265.6 g mol^{-1}).

For Fe_3DAS_6 complex, under O_2 and N_2 atmospheres, the TG/DTG curves keep the same previous characteristics. The first mass losses in both experimental curves have a different percentage of 15.43% (O_2) and 15.35% (N_2). However, under N_2 atmosphere, there is a shorter temperature range centered on 118 °C, differently from the mass loss under O_2 (40–100) °C. The both simulations refer to the release of hydration water molecules and the apparent beginning of thermal decomposing of the compound (under N_2 and O_2). For other temperatures, it is seen that up to 500 °C all the complex is decomposed under O_2,

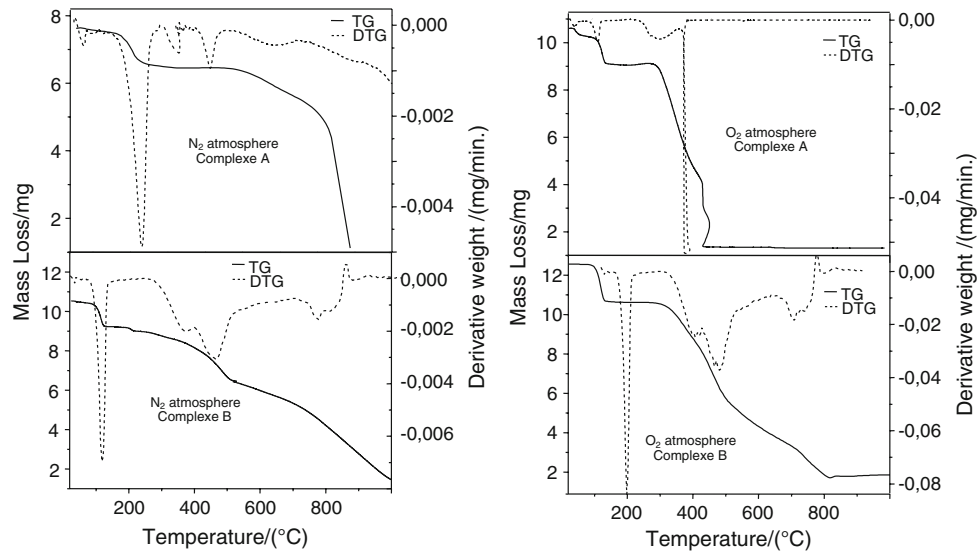

Fig. 4 TG/DTG curves of the complexes A and B, under dynamic O_2 and N_2 atmospheres

Table 3 Summarized TG/DTG data and mass-loss tentative assignments of complex Fe_2DAS_4 under flow N_2 (a) and O_2 (b)

Complex	Temperature/°C	Assignment	Experimental (calculated) mass loss/%
(a)	(40–120)	Loss of 9 H_2O	12.30 (12.80)
	(120–459)	Loss of [$C_{12}H_{10}N$], 3 SO_2	27.31 (28.45)
	(560–1000)	Loss of 3 [$C_{12}H_{10}N$], SO_3	46.57 (46.14)
		Residue Fe_2O_3	13.82 (12.61)
(b)	(120–480)	Loss of 7 H_2O, SO_2	14.71 (15.00)
	(505–515)	Loss of 4 [$C_{12}H_{10}N$], 2 SO_2, SO_3, 2 H_2O	72.65 (72.38)
		Residue Fe_2O_3	12.64 (12.62)

Table 4 Summarized TG/DTG data and mass-loss tentative assignments of Fe_3 DAS_6 under flow N_2 (a) and O_2 (b)

Complex	Temperature/°C	Assignment	Experimental (calculated) mass loss/%
(a)	(40–118)	Loss of 12 H_2O, SO_2	15.35 (14.96)
	(300–400)	Loss of [$C_{12}H_{10}N$], 2 SO_2	14.99 (15.82)
	(401–690)	Loss of 4 [$C_{12}H_{10}N$], 1 SO_3	41.09 (40.18)
	(700–1000)	Loss of 1[C_{12} $H_{10}N$], 1SO_2, 1SO_3	15.63 (16.67)
		Residue Fe_3O_4	12.94 (12.37)
(b)	(40–100)	Loss of 12 H_2O, SO_2	15.43 (14.96)
	(105–500)	Loss of 6 [$C_{12}H_{10}N$], 3SO_2, 2 SO_3	72.10 (72.67)
		Residue Fe_3O_4	12.47 (12.37)

while under N_2 atmosphere; the mass losses are extended up to 1000 °C. The both residues of mass losses simulation in O_2 (12.37%) and N_2 (12.37%) resulted in the Fe_3O_4. The percentage values led to the calculation of molecular mass of the Fe_3DAS_6 complex as 1870.7 g/mol (O_2) and (N_2) (elemental analysis 1871.4 g/mol^{-1}).

Characterization of oxides from the thermal treatment of the Fe_xDAS_{2x} complexes

The product of thermal decomposition of the Fe_2DAS_4 complex presents an XRD with band lines located at 2 θ: 24.2, 33.2, 35.8, 40.9, 49.5, 54.1, 62.6, 64.1 (Fig. 6) and

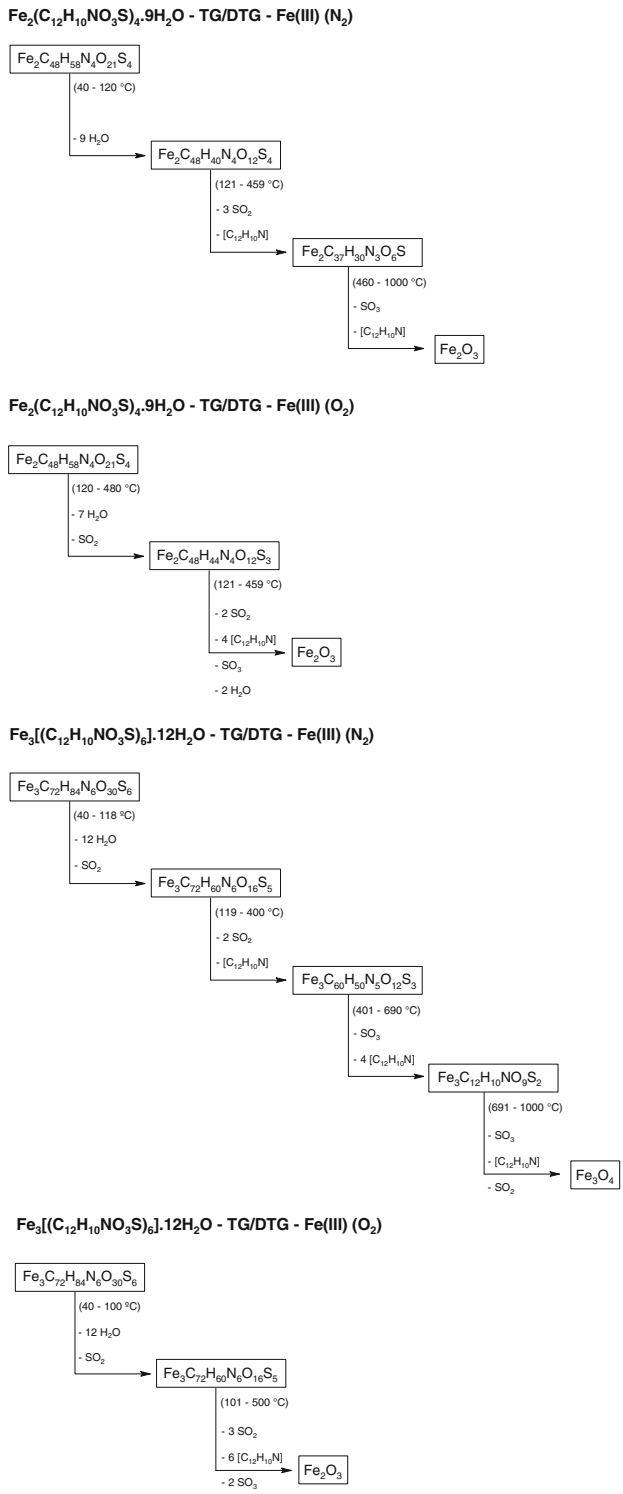

Fig. 5 Scheme of TG/DTG mass losses corresponding to Tables 3 and 4

attributed to the phase α-Fe_2O_3 (Fig. 6) [7, 8, 23–25]. The same way, the residue of the complex Fe_3DAS_6 sample showed band lines at 2 θ: 37.9, 44.0, 64.3, 77.4 attributed to phase Fe_3O_4 (Fig. 6) in accordance with literature data

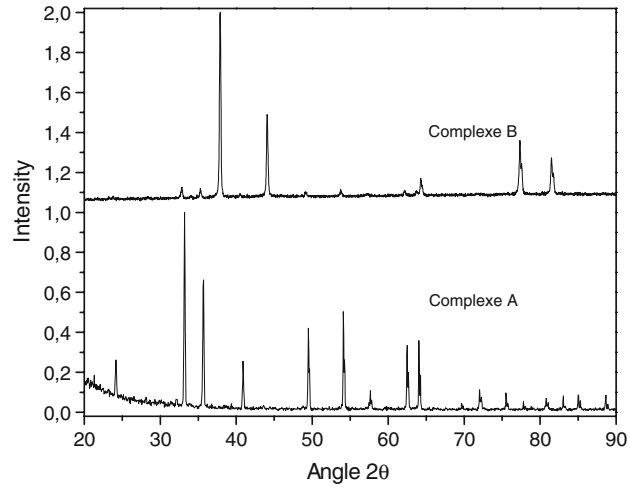

Fig. 6 XRD patterns of the residues of complexes A and B

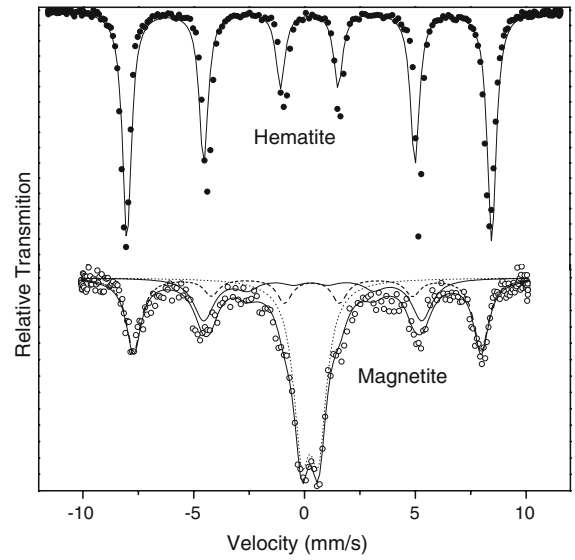

Fig. 7 ^{57}Fe-Mössbauer spectrum of α-Fe_2O_3 and Fe_3O_4

[3, 4, 6, 23–25]. The XRD attributions confirmed the results found in the TG/DTG analyses.

Figure 7 shows the ^{57}Fe Mössbauer spectra (room temperature) of α-Fe_2O_3 and Fe_3O_4 obtained in the thermal decomposition of the Fe_2DAS_4 and Fe_3DAS_6 complexes, respectively [3, 19].

α-Fe_2O_3 is constituted of dense packing oxygen cells where Fe^{3+} ions occupy O_h sites manifesting paramagnetic characteristics when at room temperature and antiferromagnetic, at low temperatures. The room temperature spectrum of α-Fe_2O_3 is represented by six lines from the hyperfine field ($\delta = 0.38$ mms^{-1} and $\Delta = +0.12$ mms^{-1}) resulting from the alignment of spins, which does not occur at low temperatures. Under these temperatures, the change in

Table 5 Mössbauer spectroscopy parameters for the Fe_3O_4 and Fe_2O_3

Compound (Fe_2O_3)	δ (mm/s)	ΔE_Q (mm/s)	BH_f (T)	τ (mm/s)	Fe (%)
	0.336	0.000	51.17	–	–
Compound (Fe_3O_4) site from Fe	δ (mm/s) isomer shift	ΔE_Q (mm/s) quadrupole splitting	BH_f (T) hyperfine field	τ (mm/s) line width	Fe (%)
Tetrahedral	0.225	0.112	48.83	0.500	26.43
Octahedral	0.554	−0.120	49.09	0.831	11.19
Doublet	0.227	0.779	0.00	0.770	62.38

the spins magnetic alignment will invert the Δ interaction value, making it negative. The temperature at which the Δ value will invert itself is called Morin [19] temperature. The α-Fe_2O_3 particle size determines the fraction of material with superparamagnetic properties originated due to the decrease in spin relaxation time. Therefore, the decrease in particle size also lowers Morin temperature when inducing the increase in surface effect and decreasing Δ interactions [3, 19].

The ^{57}Fe Mössbauer spectra of α-Fe_3O_4 at room temperature obtained from a sample of Fe_3DAS_4 thermally treated in air contains six resulting lines of a hyperfine field of 51.17 T with ($\delta = 0.34$ mms^{-1} and $\Delta = 0.0$) (Fig. 7). Comparing this α-Fe_2O_3 spectrum to the ones that show the effect of variation of the sizes of the particles, it is noticed a close similarity to the one that refers to samples of α-Fe_2O_3 with the sizes up to 15 nm and that have a high content of super paramagnetic fraction [3, 19]. On the contrary, the spectrum of ^{57}Fe Mössbauer of Fe_3O_4 at room temperature obtained from $Fe_3(DAS)_6$ thermally treated in air contains many singularities [3, 19]. Magnetite has been described as a spinoidal structure Fe^{2+} (A) [Fe^{3+}] (B) O_4, in which Fe^{2+} ions occupy the tetrahedral (T_d) site (A) and the octahedral (O_h) site (B) contain the Fe^{2+} Fe^{3+} ions. However, the temperature above 77 K (Verwey temperature) starts in the T_d site A, the process of oxidation and electronic transference: $Fe^{2+} \rightarrow Fe^{3+} + e^-$. Those electrons move towards the interstices B in a way that $Fe^{3+} + e^- \rightarrow Fe^{2+}$. The vacancies in the O_h sites (B) will be occupied by an equal number of Fe^{2+} and Fe^{3+} ions. Site A starts to be mainly occupied by Fe^{3+} ions. At 300 K, for example, the exchange of electrons is very fast and produces a balanced spectrum with a sextet without quadrupole [3, 19]. In samples that were submitted to heating above that temperature and/or to oxidation processes, the O_h site A is occupied by Fe^{3+} ions and site B can be occupied by Fe^{2+} (inverted spinel) or by a mixture of Fe^{2+} and Fe^{3+}, depending on the conditions of treatment of the sample [3, 19, 25].

The Fe_3O_4 resulting from heating the precursor A to 1000 °C, under atmospheric air, presented the Mössbauer spectrum with two sextets and one doublet. The spectrum analysis reveals that the first sextet (broken spectrum) can be associated to the occupation of the T_d site A by the Fe^{3+} ions ($\delta = 0.225$ mms^{-1} and $\Delta = 0.112$ mms^{-1}). A second sextet (continuous) refers to the O_h site B, occupied by Fe^{2+} ($\delta = 0.564$ mms^{-1} and $\Delta = -0.120$ mms^{-1}). The doublet corresponds to the occupation of the site A by the Fe^{3+} in a cubic tetrahedrically distorted system ($\delta = 0.227$ mms^{-1} and $\Delta = 0.779$ mms^{-1}). These data show that, possibly, the Fe_3O_4 spinel produced in this work is inverted [3, 19]. However, there is an intriguing point in this occupation. The total percentage of the Fe^{3+} in the various sites is 88.81%, distributed in such a way that 26.43% of the ions are responsible for a hyperfine T_d field of 48.83 T in A, while 62.38% are responsible for a null hyperfine field resulting from T_d distortion in site B. This unbalanced occupation of the ions contained in the site could have been caused by difficulties in the process of electronic transference from site A to site B. The latter contains only 11.19% of Fe^{2+}. The values of δ that were lower than the prevision indicating that an incomplete electronic transference occurs and stresses the unbalance of the inverted magnetite [3, 19]. However, the little participation of the Fe^{2+} ions in site B can be connected to a possible process of stabilization of the Fe^{3+} ion. The values for the hyperfine fields of the samples that were studied showed to be higher than the ones of the common magnetite as well as the line widths for the T_d field from 0.50 to 0.83 mm/s for the O_h field are much higher than the traditional (0.19 mm/s). As mentioned, it seems reasonable that a distribution of hyperfine fields on the surface of the ultra fine magnetic particles would be able to induce an increase in the contribution of the demagnetization for the total field in the micro crystals. This evidence seems to be a reasonable explanation and it is supported in the data in Table 5, where the larger fraction of those nanoparticles (62.38%) occupies a tetrahedrically distorted place where they present superparamagnetic characteristics [3, 19].

Conclusions

In this study, the anionic surfactant was put to interact with the Fe atom allowing to DAS ligand two possible alternatives: the complexation or reduction. In reaction 1, the

Fe(III) is reduced to Fe(II) due to the excess of DAS. In the oxidizing degradation, the excess of surfactant was consumed. The conclusion is that the complexation would be sufficiently strong with Fe(II) ion, however, if there are ions Fe(III) in aqueous solution, the reduction would overcome.

The TG/DTG data contributed to investigate the stability of the two Fe(II) complexes relatively to the oxidation in O_2 atmosphere. As is seen, the total thermal decomposition of the two complexes is completed before 500 °C. However, the starting temperature of the thermal decomposition (120 °C) is much lower for the Fe_2DAS_4 compound, than it is for the Fe_3DAS_6, where only water loss is observed to 200 °C. This question seems to have a more affirmative answer if the products of TG/DTG and the thermal treatment are investigated. The thermal decomposition product of the Fe_2 DAS_4 is α-Fe_2O_3 while the one obtained from Fe_3 $(DAS)_6$ refers to magnetite, Fe_3O_4. The obvious conclusion is that the Fe_2 DAS_4 compound containing Fe(II), reduced by the DAS surfactant, is in a reasonable level of instability and when treated under an oxidizing atmosphere, it produces an oxide that contains only Fe(III) ion.

References

1. Zhonghua W, Lin G, Qianshu L, et al. Surface atomic structures of Fe_2O_3 nanoparticles coated with cetyltrimethyl ammonium bromide and sodium dodecyl benzene sulphonate: an extended x-ray absorption fine-structure study. J Phys: Condens Matter. 1999;11:4961–70.
2. Yoon CS, Lim SK, Chung KJ, et al. Synthesis of iron oxide nanoparticles in a polymide matrix. J Colloid Interface Sci. 2004;273:517–22.
3. Panda RN, Gajbhiye NS, Balaji G. Magnetic properties of interacting single domain Fe_3O_4 particles. J Alloys Compd. 2001;326:50–3.
4. Jiang L, Sun W, Kim J. Preparation and characterization of w-functionalized polystyrene-magnetite nanocomposites. Mater Chem Phys. 2007;101:291–6.
5. Korolev VV, Arefyev IM, Blinov AV. Heat capacity of superfine oxides of iron under applied magnetic fields. J Therm Anal Cal. 2008;92:697–700.
6. Chen Q, Wang J, Sun J, et al. One-step hydrothermal process to prepare highly crystalline Fe_3O_4 nanoparticles with improved magnetic properties. Mater Res Bull. 2003;38:1113–8.
7. Lu J, Fan J, Xu R, Roy S, et al. Synthesis of alkyl sulfonate/alcohol-protected y-Fe_2O_3 nanocrystals with narrow size distributions. J Colloid Interface Sci. 2003;258:427–31.
8. Liu H, Wei Y, Sun Y. The formation of hematite from ferrihydrite using Fe(II) as a catalyst. J Mol Catal A-Chem. 2005;226:135–40.
9. Mailhot G, Asif A, Bolte M. Degradation of sodium 4-dodecylbenzenesulphonate photoinduced by Fe(III) in aqueous solution. Chemosphere. 2000;41:363–70.
10. Horváth O, Bodnár E, Hegyi J. Photoassited oxidative degradation of surfactants and simultaneous reduction of metals in titanium dioxide dispersions. Colloids Surf A: Physicochem Eng Asp. 2005;265:135–40.
11. Ciesla P, Kocot P, Mytych P, Stasicka Z. Homogeneous photocatalysis by transition metal complexes in the environment. J Mol Catal A: Chem. 2004;224:17–33.
12. Rose AL, Waite TD. Role of superoxide in the photochemical reduction of iron in seawater. Geochim Cosmochim Acta. 2006;70:3869–82.
13. Zuo Y, Zhan J. Effects of oxalate on Fe-catalyzed photooxidation of dissolved sulfur dioxide in atmospheric water. Atmos Environ. 2005;39:27–37.
14. Beentjes PCJ, Van Den Brand J, De Wit JHW. Interaction of ester and acid groups containing organic compouds with iron oxide surfaces. J Adhesion Sci Technol. 2006;20:1–18.
15. Zhang H, Wen X, Wang Y. Synthesis and characterization of sulfate and dodecylbenzenesulfonate intercalated zinc-iron layered double hydroxides by one-step coprecipitation route. J Solid State Chem. 2007;180:1636–47.
16. Nakanishi K, Solomon PH. Infrared absorption spectroscopy. 2nd ed. San Francisco, CA: Holden-Day; 1977.
17. Bellamy LJ. The infrared spectra of complex molecules. Vol. 2. London: Chapman and Hall; 1980.
18. Xu ZP, Braterman PS. High affinity of dodecylbenzene sulfonate for layered double hydroxide and resulting morphological changes. J Mater Chem. 2003;13:268–73.
19. Greenwood NN, Gibb TC. Mössbauer spectroscopy. New York: Barnes and Noble Inc; 1971.
20. Machado LC, Marins AAL, Muri EJB, et al. Reaction products between sodium diphenyl-amine-4-sulfonate and hydrated $LaCl_3$: thermogravimetric and spectroscopic study. J Therm Anal Cal. 2004;75:615–21.
21. Crepaldi LE, Pavan PC, Tront J. Chemical, structural, and thermal properties of Zn(II)-Cr(III) layered double hydroxides intercalated with sulfated and sulfonated surfactants. J Colloid Interface Sci. 2002;248:429–42.
22. Zhang LH, Jiang H, Gong H, Sun ZL. Characteristics of thermal decomposition products of rare earth, alkali earth metal and transition metal p-toluenesulfonates. J Therm Anal Cal. 2005;79:731–5.
23. JCPDS—International Centre for Diffraction Data 1996.
24. Guinier A. X-ray diffraction in crystals, imperfect crystals and amorphous bodies. New York: Dover Publications; 1994.
25. Korolev VV, Arefyev IM, Ramazanova AG. The magnetocaloric effect of superfine magnets. J Therm Anal Cal. 2008;92:691–5.